AIMS Energy, 3(4):525-546.
DOI: 10.3934/energy.2015.4.525
Received date 5 June 2015,
Accepted date 22 September 2015,
Published date 25 September 2015

http://www.aimspress.com/

Research article

Numerical comparison between deep water and intermediate water depth expressions applied to a wave energy converter

Pedro Beirão [1,2,*] and Duarte Valério [2]

[1] Instituto Politécnico de Coimbra, ISEC, DEM, Coimbra, Portugal
[2] LAETA, IDMEC, Instituto Superior Técnico, Universidade de Lisboa, Lisboa, Portugal

* **Correspondence:** Email: pbeirao@isec.pt; Tel: +351 239 790 332;
Fax: +351 239 790 331.

Abstract: The energy that can be captured from the sea waves and converted into electricity should be seen as a contribution to decrease the excessive dependency and growing demand of fossil fuels. Devices suitable to harness this kind of renewable energy source and convert it into electricity—wave energy converters (WECs)—are not yet commercially competitive. There are several types of WECs, with different designs and working principles. One possible classification is their distance to the shoreline and thus their depth. Near-shore devices are one of them since they are typically deployed at intermediate water depth (IWD). The selection of the WEC deployment site should be a balance between several parameters; water depth is one of them. Another way of classifying WECs is grouping them by their geometry, size and orientation. Considering a near-shore WEC belonging to the floating point category, this paper is focused on the numerical study about the differences arising in the power captured from the sea waves when the typical deep water (DW) assumption is compared with the more realistic IWD consideration. Actually, the production of electricity will depend, among other issues, on the depth of the deployment site. The development of a dynamic model including specific equations for the usual DW assumption as well as for IWD is also described. Derived equations were used to build a time domain simulator (TDS). Numerical results were obtained by means of simulations performed using the TDS. The objective is to simulate the dynamic behavior of the WEC due to the action of sea waves and to characterize the wave power variations according with the depth of the deployment site.

Keywords: wave energy converter; deep water; intermediate water depth; relative depth criterion; dynamic model; simulation

1. Introduction

In the last decades, wave energy is being considered as a valid alternative for the production of electricity in order to deal with the growing energy demand. Besides that, energy production from fossil fuels is contributing to serious environmental problems. Since the oceans cover the most part of the earth's surface, there is a vast amount of energy available in the oceans to be exploited and to satisfy the needs of the world energy consumption. Additionally their power density is higher than that of the most developed renewable energies. Energy may be extracted from the ocean thanks to its thermal energy, to tides, and to waves, which are the object of this paper. However electricity production will depend on the wave energy available at the deployment site, since wave climates sometimes may vary significantly with short distances.

There are several ways to distinguish the different concepts of different WECs, whereby they are able to extract energy from sea waves and convert it into electricity. Up till now many prototypes with different designs and working principles were conceived, developed and tested, but only a few of them have reached a commercial stage [1–3].

They can be classified according with their energy-extracting method, size and distance to the shoreline. Using this last criterion, which is related with the WEC deployment site (and thus its depth), they can be divided in shoreline, near-shore and offshore devices [1–4]. Near-shore devices are typically deployed at IWD.

Special attention should be given to the WEC deployment site, since among other issues the depth effect could affect their wave power capture performance. When in the project stage WECs are usually designed for DW deployment. The major advantage is that the wave power that is expected to be harnessed will be higher when compared with IWD locations. However, the WEC ability to deal with extreme wave load conditions as well as economic issues (significant costs in installation, maintenance, access to the device, among others) should not be put aside. If an IWD location is selected instead, less energetic waves are to be expected. They will lead to a reduction in the captured wave power. In contrast, structural and other costs will decrease. So the ultimate selection of the WEC deployment site should be a balance between several parameters (design, logistic, environmental, etc.). These concerns are widespread in the literature and shared by several authors [4–7]. In [4] the effect of finite water depth upon the wave energy captured by a floating point absorber is assessed. Emphasis is put on wave spectral models that take into account deep water and finite depth. A case study for a location in the west coast of Portugal is presented. In [5] a study is described of the effect of the water depth on the wave energy resource. Attention is put on a given depth range (50 to 30 meters) as well as on the dependency of a set of variables (slopes, bottom roughness and wave directions). They use a third-generation spectral wave model to simulate waves. A case study for the north coast of Cornwall, in United Kingdom is also presented. In [6] is analyzed the wave climate transformation from the offshore until the nearshore of the western coast of Orkney, in Scotland. The authors also showed that the way wave power is defined can have an effect on the apparent difference in wave power at shallower depths. More recently, in [7], the authors present a detailed study including experimental tests performed in an artificial shallow water wave basin using a large array of heaving point absorber WECs for a range of regular and irregular waves.

Considering a near-shore floating point WEC, this paper focuses on the numerical study, by means of simulations, of the differences arising in the wave power that can be captured when the typical DW assumption is compared with the most realistic IWD consideration. A parameter known as the Relative

Depth Criterion (RDC) is responsible by the selection between DW and IWD equations respectively. The development of a mathematical model with specific equations for the usual deep water assumption as well as for intermediate water depth is also described. The objective is to simulate the dynamic behavior of the WEC due to the action of sea waves.

The following section characterizes in brief the floating point absorber WEC equipped with an electric linear generator (ELG) assumed as being the power take off (PTO) of the device. Still, the conclusions also apply to WECs that use a hydraulic PTO. Section 3 details the WEC dynamic model including the derivation of several equations for the considered forces, taking into account the deployment of the device in deep water as well as in intermediate water depth. Section 4 describes the wave data used as an input in the TDS simulator addressed in section 5. Results are presented in an independent section. The last section outlines the principal conclusions.

2. WEC characterization and working principle

The design of the WEC adopted for this study fits in the floating point absorber category since its characteristic dimension (diameter) has a negligible size when compared to the ocean wavelength [2,3,8]. This design was chosen due to its simple geometry, relatively easy to model dynamic behavior and its capacity for capturing wave energy per a wider wave front when compared with its own characteristic dimension [3]. Detailed literature reviews about this kind of WEC may be found, for instance, in [1–3]. If it is assumed that this WEC is deployed at an intermediate water depth it can also be classified as a near-shore device. A point absorber is typically a single body that converts the wave energy using the heave motion by reacting against stationary base placed at the seabed [9]. The components of the PTO system could be enclosed in the sealed waterproof concrete mooring foundation placed at the seabed.

It is assumed that the WEC converts wave energy due to the relative motion between a floating buoy and the stationary seabed mooring. Therefore, the two main components are a cylindrical buoy, which floats with the sea waves, which is assumed rigidly connected to a heaving piston. Although the motion of a point absorber may have six degree modes [4,8], due to simplicity reasons the floating buoy is assumed to oscillate only in heave mode. The working principle is quite simple: the successive wave crests and troughs cause the heave motion of the buoy connected to the piston. The buoy floats and moves upwards under the influence of a wave crest and moves downwards under the effect of a wave trough.

In order to convert the energy available from the sea waves into electricity, WECs must have some kind of mechanism, known as PTO, by which energy is transferred between the waves and the device itself. In this particular situation, the relative heave motion between the two main WEC components will be directly converted into electrical energy by an ELG mainly constituted by a translator, traveling with the piston, and a stator. Therefore when the buoy moves in the waves, so does the piston and the translator placed inside the stator [10].

3. WEC dynamic model

The objective is to develop a dynamic model of the WEC following, for instance, the work presented in [1–3,8,9,11–13]. It describes analytically the buoy heave motion with respect to its acceleration and is based on the second Newton's law.

An ideal fluid with irrotational motion is assumed [9] so viscous effects are neglected [14]. Additionally, wave amplitudes and oscillations are sufficiently small when compared with the wavelength. Hence linear potential wave theory is used to describe the hydrodynamic behavior [3,8].

However, instead of the most common assumption of deep water, specific equations will also be derived for intermediate water depth, which is a more realistic approach for this near-shore WEC design.

The total external force f_{ext} acting vertically on the buoy results from the sum of several components:

$$\sum f_{ext}(t) = m.\ddot{z}(t) \tag{1}$$

where m is the mass and $\ddot{z}$ is the corresponding vertical acceleration component with respect to time t.

In equation (1) f_{ext} includes the vertical components of the hydrodynamic viscous drag force f_v, the hydrostatic buoyancy force f_b exerted on the buoy due to the instantaneous buoy position with respect to the seawater free surface, the end stop spring force f_{es} that limits the stroke of the piston that moves the translator of the ELG, the PTO force f_{PTO}, and the wave force f_w. This wave force may be decomposed in two hydrodynamic components acting upon the wetted buoy surface [1,8]: the heave excitation force f_{exc} due to the incident waves acting upon the assumed stationary buoy and the radiation force f_r due to the energy transfer from the heaving buoy to the waves that are radiated away from the buoy.

The linearized time-domain motion equation (1) of the heaving floating point WEC can be rewritten similarly to several others that, for instance, may be found in [2,11,12]:

$$\begin{aligned}(m_b + m_a).\ddot{z}(t) &= -f_v(t) - f_b(t) + \left[f_{exc}(t) - f_r(t) \right] - f_{es}(t) - f_{PTO}(t) \\ (m_b + m_a).\ddot{z}(t) &= -f_v(t) - C.z(t) + \left[f_{exc}(t) - Z.\dot{z}(t) \right] - f_{es}(t) - f_{PTO}(t)\end{aligned} \tag{2}$$

where m_b and m_a are the buoy and added masses respectively and z is the buoy displacement.

Considering a cylindrical buoy of radius r, masses m_b and m_a [15] are respectively given by:

$$m_b = \rho_b.V_b \Leftrightarrow m_b = \rho_b.\pi.r^2.h \tag{3}$$

$$m_a = \frac{1}{2}.\rho_w.V_b \Leftrightarrow m_a = \frac{1}{2}.\rho_w.\pi.r^2.h \tag{4}$$

where ρ_b is the buoy density, V_b is the buoy volume, h is the buoy height and ρ_w is the seawater density.

3.1. Hydrodynamic viscous drag force

The hydrodynamic viscous drag force f_v should not be neglected since the generated viscous damping effect is responsible by a realistic WEC response and power extraction performance, as pointed out in [1].

In equation (2), according with [16] and resorting to the Morison equation [17], the hydrodynamic viscous drag force f_v is a damping force that may be given by:

$$f_v(t) = \frac{1}{2}.C_d.\rho_w.A_{proj}.w(t).|w(t)| \tag{5}$$

where C_d is the drag coefficient, A_{proj} is the projected area of the buoy normal to the flow and w is the vertical component of the undisturbed fluid velocity relative to the buoy.

A parameter known as the RDC is responsible by the selection between DW and IWD equations. The RDC is defined as the quotient between the water depth d_w and the wavelength λ [17]. When this parameter is higher than 1/2 [17], DW (also known as infinite water depth) equations should be used.

Therefore, assuming DW, the fluid velocity w is given by [17]:

$$w(t) = \frac{\pi.H}{T_w} e^{\left(\frac{2\pi.d}{\lambda}\right)}.\sin(\omega.t) \tag{6}$$

where H is the wave height, T_w is the wave period, d is the distance above sea water level (SWL) and ω is the wave angular frequency. For DW, the wavelength λ and the wave angular frequency ω are respectively given by [16]:

$$\omega = \frac{2\pi}{T_w} \tag{7}$$

$$\lambda = \frac{g.T_w}{\omega} \tag{8}$$

where g is the acceleration due to gravity.

For IWD (where RDC ranges from 1/25 to 1/2 [16]), the fluid velocity w is given by [16]:

$$w(t) = \frac{H.g.T_w}{2.\lambda}.\frac{\sinh\left[\frac{2\pi.(d+d_w)}{\lambda}\right]}{\cosh\left[\frac{2\pi.d_w}{\lambda}\right]}.\sin(\omega.t) \tag{9}$$

where $(d+d_w)$ is the distance above the seabed. The wave angular frequency ω may be computed from the dispersion equation considering IWD [3]:

$$\omega^2 = g.k.\tanh(k.d_w) \tag{10}$$

where k is the wave number and the wavelength λ is now given by [16]:

$$\lambda = \frac{g.T_w}{\omega}.\tanh(k.d_w) \tag{11}$$

An alternative equation for λ considering also IWD may be provided by [16]:

$$\lambda \approx \frac{g.T_w^2}{2\pi}.\sqrt{\tanh\frac{4\pi^2.d_w}{g.T_w^2}} \tag{12}$$

This approximation explicitly gives λ in terms of T_w and is sufficiently accurate for many engineering calculations. A maximum error of 10% occurs when the RDC is equal to 1/2 [16].

3.2. Hydrostatic buoyancy force

In equation (2), C is the restoring or stiffness coefficient accounting for the instantaneous buoy position with respect to the undisturbed free seawater surface [2]. If C is considered a linear coefficient, $C.z$ corresponds to the hydrostatic buoyancy (restoring or stiffness) force f_b exerted on the buoy due to the instantaneous buoy position with respect to the seawater free surface. It may be given by:

$$f_b(t) = C.z(t) \Leftrightarrow f_b(t) = [\rho_w.g.A_b].z(t) \tag{13}$$

where A_b is the buoy cross-sectional area.

3.3. End stops spring force

In order to prevent the WEC to be damaged when the incident waves are too high, end stops springs are used to limit the stroke of the piston. The end stops spring force f_{es} may be decomposed

into an upper end stop force f_{es_u} and lower end stop force f_{es_l}, modelled as in [18,19]:

$$f_{es_u}(t) = \begin{cases} -k_u.\left[z(t) - l_u\right], & z(t) > l_u \\ 0, & z(t) \le l_u \end{cases} \tag{14}$$

$$f_{es_l}(t) = \begin{cases} -k_l.\left[l_l + z(t)\right], & z(t) < -l_l \\ 0, & z(t) \ge -l_l \end{cases} \tag{15}$$

where k_u and k_l are respectively the upper and lower end stops spring constants and l_u and l_l are respectively the lengths from the upper and lower end stops springs [18].

3.4. Excitation force

In equation (2), the heave excitation force f_{exc} can be obtained based in [3,20]:

$$f_{exc}(t) = \left|f_{exc}\right|.\cos(\omega.t + \theta) \tag{16}$$

where $\theta \approx 0$ for a heaving floating body of the point absorber type [5]. The amplitude of the heave excitation force $\left|f_{exc}\right|$ can be computed from [3,20]:

$$\left|f_{exc}\right| = \kappa_3.\rho_w.g.\frac{H}{2}.\pi.r^2 \tag{17}$$

where κ_3 is the heave excitation force coefficient. The evolution of this hydrodynamic parameter depends of the product between the wave number k and the cylindrical buoy radius r. Values of κ_3 were obtained from [3].

3.5. Radiation force

In equation (2), Z is the heave radiation impedance (also known as radiation damping coefficient) accounting for the buoy damping due to the transfer of energy to the waves radiated away from the buoy when it heaves [2]. Assuming that the buoy behaves like a semi submerged cylinder of radius r on deep water this parameter may be given by [3]:

$$Z = \frac{1}{2}.\rho_w.\pi.r^2.h.\omega.\left(\varepsilon_{33} + i\mu_{33}\right) \Leftrightarrow Z = R_{33} + i\omega.m_{33} \tag{18}$$

where R_{33} or ε_{33} and m_{33} or μ_{33} are respectively the non-dimensional heave radiation

resistance and added mass coefficients. These hydrodynamic parameters also depend on the product between the wave number k and the cylindrical buoy radius r.

If the heave radiation impedance Z is considered a linear damping coefficient, $Z.\dot{z}$ corresponds to the radiation force f_r that can be derived following [3]. Actually f_r is a damping force which can be given by:

$$f_r(t) = Z.\dot{z}(t) \Leftrightarrow f_r(t) = \left[R_{33} + i\omega.m_{33}\right].\dot{z}(t) \tag{19}$$

For IWD, equation (19) is no longer valid, mainly due to changes in the radiation resistance coefficient R_{33}. Therefore an alternative equation for R_{33} must be found. Considering a heaving axisymmetric body with a hemi cylindrical bottom, R_{33} is related with the amplitude of the heave excitation force $\left|f_{exc}\right|$ by [3]:

$$R_{33} = \frac{k}{8.J}.\left|f_{exc}\right|^2 \tag{20}$$

where the (time averaged) wave power level (power per unit width) J for an incident sinusoidal wave with height H is given by [3,21]:

$$J = \frac{\rho_w.g^2.\left|H\right|^2}{16.\omega}.D\left(k.d_w\right) \tag{21}$$

where $D\left(k.d_w\right)$ is the so-called depth function given by [3]:

$$D\left(k.d_w\right) = \left(1 + \frac{4.k.d_w.e^{-2.k.d_w}}{1-e^{-4.k.d_w}}\right).\frac{1-e^{-2.k.d_w}}{1+e^{-2.k.d_w}} \tag{22}$$

Alternative equations for $D\left(k.d_w\right)$ may also be found in [3,16].

3.6. PTO force

Wave energy is transferred between the sea waves and the WEC trough the PTO, assumed to be an ELG. The main components of the ELG are a translator attached to the piston and a stator. When the buoy moves with the waves, so does the piston and the translator placed inside the stator. The objective is to convert the relative heave motion between these two components into electricity. The PTO is the mechanism responsible for this direct conversion.

The equation modelling the ELG follows [14,18,19,22], and is derived as a mechanical damping function dependent on the velocity [18] and displacement of the piston.

The computation of the voltage V at the terminals of each one of the three phases of the ELG

follows the analytical model originally presented in [22] and adopted also by [12]:

$$V(t) = \frac{2\pi.B_t.w_t.d_s.p.q.c}{w_p}.\dot{z}(t).\sin\left(\frac{2\pi}{w_p}.z(t) - \delta\right) \tag{23}$$

where B is the magnetic field in a tooth, w_t is the width of a stator tooth, d_s is the width of the stator stack, p is the total number of poles, q is the number of slots per pole and phase, c is the number of cables in a slot, w_p is the pole pair width and δ is the load angle [22].

Assuming a resistive load R_l one of the possible equations for the electrical power P at each phase of the ELG is given by:

$$P(t) = \frac{\left[V(t)\right]^2}{R_l} \tag{24}$$

The buoy position will affect the piston and consequently the translator position. When the translator overlaps the stator the electrical power production will change accordingly with the ELG active area A_a since the stator area will not be 100% active for all translator positions [14]. It is expected that the ELG performance decreases when the ELG active area A_a decreases [14].

The ELG active area A_a is given by [18,19]:

$$A_a = \begin{cases} 0, \ if \ |z(t)| \geq \frac{1}{2}.(l_t + l_s) \\ 1, \ if \ |z(t)| \leq \frac{1}{2}.(l_t - l_s) \\ \frac{1}{l_s}.\left[\frac{1}{2}.(l_t + l_s) - |z(t)|\right], \ else \end{cases} \tag{25}$$

where l_t and l_s are the length of the translator and stator respectively.

In equation (2), the conversion from mechanical to electrical energy is given by the PTO force f_{PTO}. This is an electromagnetic damping force [19] that counteracts the buoy heave motion and is given by [12,19] (an alternative formulation may be found in [18]):

$$f_{PTO}(t) = \frac{\overline{\sum_{i=1}^{3} P_i(t)}}{\dot{z}(t)}.A_a(t) \tag{26}$$

4. Wave data

Statistical wave data to characterize the Portuguese wave climate is available with the ONDATLAS software. It assesses the wave energy available along the Portuguese coast using information from several buoys placed at different locations of the Portuguese shore [23].

The data chosen for this study was obtained from the Leixões-buoy site, at 41°12.20′N; 9°5.30′W [24–26], located near the Aguçadoura Wave Farm. This was the world's first wave farm where three Pelamis WECs were deployed and tested.

Irregular wave data retrieved from this location was used as an input in the TDS in order to perform several simulations. Real sea waves are not sinusoids. They can be decomposed as a sum of sinusoids, with a spectrum $S(\omega)$ giving the importance of the contribution of each frequency ω (in rad/s) [3].

The significant wave height H_s is related to the spectrum by [25]:

$$H_s = 4\sqrt{\int_0^{+\infty} S(\omega)\, d\omega} \tag{27}$$

Given an irregular wave with a certain power, the wave energy period T_e of a regular wave of height H_s carrying the same power is given by [25]:

$$T_e = 2\pi \frac{\int_0^{+\infty} \frac{S(\omega)}{\omega} d\omega}{\int_0^{+\infty} S(\omega)\, d\omega} \tag{28}$$

Twelve sea states (one for each month of the year), generated using H_s values from Table 1 together with Pierson Moskowitz's spectrum were devised. This spectrum models the behavior of real sea waves in the Northern Atlantic Ocean [24–26]. This one-parameter spectrum was chosen, rather than two-parameters spectra such as the Bretschneider or the Jonswap spectra, due to the Atlantic location and because calculations are simpler. The corresponding data about significant wave height H_s and values of the wave energy period T_e is given in Table 1.

Table 1. Irregular wave data used in the simulations.

	Jan	Feb	Mar	Apr	May	Jun	Jul	Aug	Sep	Oct	Nov	Dec
H_s (m)	3.2	3.0	2.6	2.5	1.8	1.7	1.5	1.9	1.9	2.3	2.8	3.1
T_e (s)	9.8	9.5	9.1	8.4	7.3	6.9	6.4	6.7	7.5	8.2	9.0	9.5

Simulations were also carried out for several regular waves. Data values for those waves, with heights H ranging from 1 to 4 m, ΔH = 0.5 m and periods T_w ranging from 6 to 12 s, ΔT_w = 0.5 s) are congruent with those given in Table 1.

5. Simulator

The TDS is an appropriate choice when dealing with irregular sea waves [2]. This is also preferable instead of a simulator in frequency domain due to the model nonlinearities [27], arising from the fact that most of the WECs are equipped with strongly nonlinear mechanisms [2]. It intends to simulate in an effective way the dynamic behavior of a floating point absorber WEC due to the action of sea waves.

The TDS was developed from the mathematical model resulting from the time domain equations derived in section 3. It was implemented in MatLab/Simulink and groups, under individual subsystems blocks shown in Figure 1, all the force equations previously derived. Another block generates the sea waves.

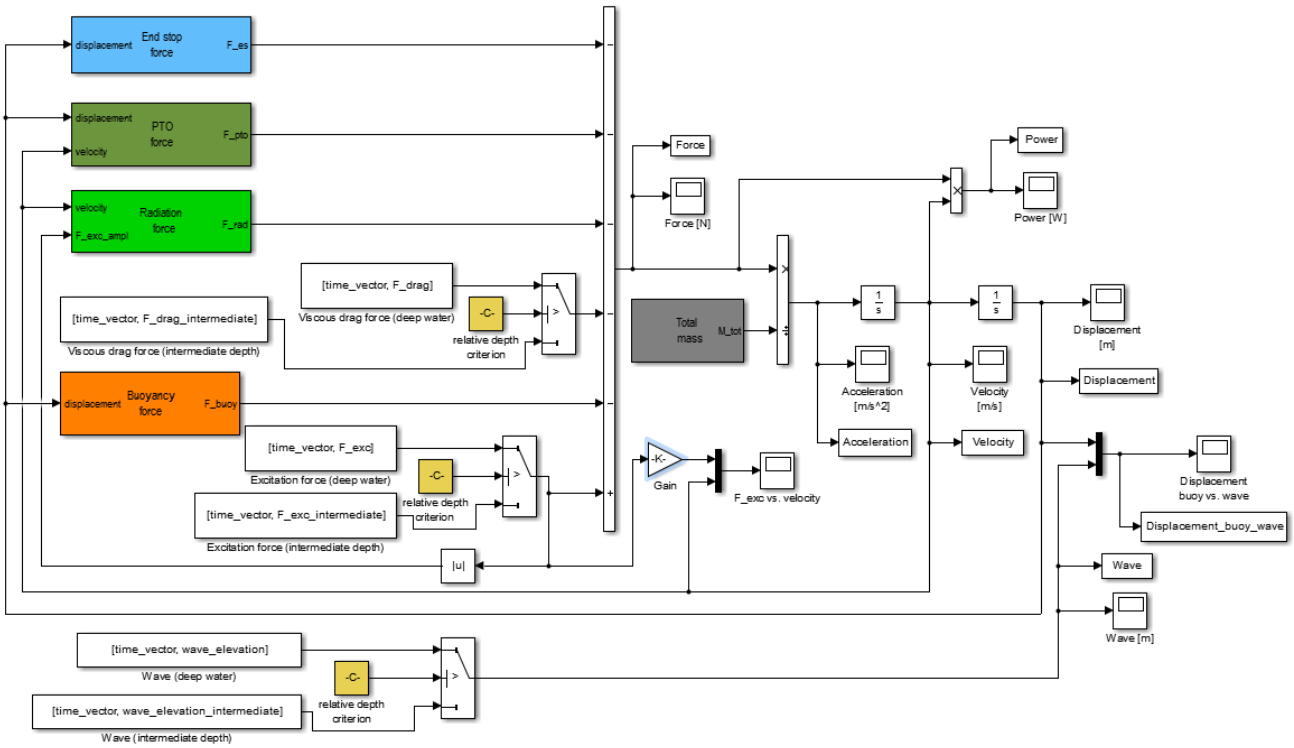

Figure 1. Dynamic model block of the TDS.

The TDS used in this work is an improved version of the one presented in [11,27]. The wave

generation block is based on so-called time domain model (TDM) simulator of the first-generation Archimedes Wave Swing (AWS) [28], and closely follows it as well as [29].

In this newer improved version the wave generation block can handle both regular and irregular waves by choosing their parameters (wave height and period for regular waves as well as the spectrum and other spectrum related values for irregular waves). Wave generation is previously made offline and then used as an input in the TDS. The Pierson-Moskowitz spectrum is used to generate a sufficiently large number of sinusoidal waves which are then summed. However DW and IWD irregular waves are different, since for IWD equations (9) to (12) are used with each sinusoidal component of the irregular wave (as done for regular waves), while for DW equation (7) is used instead.

The TDS takes into account both the usual DW as well as the more realistic IWD assumptions. The RDC is used as a trigger input and automatically allows the selection, between those two assumptions, of which specific equations should be used. Figure 2 exemplifies this procedure.

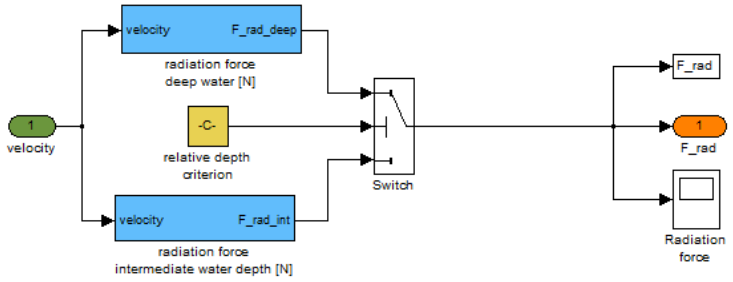

Figure 2. Selection procedure between DW and IWD.

Several other inputs, some of them resumed in Table 2, are needed to run the simulation.

Table 2. Parameters used in the TDS.

Parameter	Value	Reference
buoy radius r	3 m	[7,8,12]
buoy height h	0.8	[7,8,12]
load resistance R_l	3.1 Ω	[16]
translator length l_t	2 m	[13]
stator length l_s	2 m	[13]
upper end stop spring constant k_u	243 kN/m	[12]
lower end stop spring constant k_s	215kN/m	[12]
upper end stop spring length l_u	1.89 m	[13]
lower end stop spring length l_l	1.89 m	[13]
magnetic field in a tooth B_t	1.55 T	[16]
stator tooth width w_t	0.008 m	[16]
stator stack width d_s	0.4 m	[16]
total number of poles p	100	[16]
number of slots per pole and phase q	6/5	[16]
number of cables in a slot c	6	[16]
pole pair width w_p	0.1 m	[16]

6. Results and Discussion

Throughout this paper, more than one hundred simulations with 300 seconds (5 minutes long), using regular and irregular waves, were made resorting to the TDS built in MatLab/Simulink and described in the previous section. Two different values for the RCD were used: an RCD equal to 0.25 was chosen to perform IWD computations; DW computations were done using a unitary RCD value. These two RCD values respect the criteria described in section 3.

6.1. Regular waves

Figures 3 and 4 refer to a wider range of results in terms of the power variation computed from simulations made from 72 regular waves (values of H and T_w agree with the range defined in section 3). Figure 3 refers to computations assuming DW formulation while Figure 4 considers IWD.

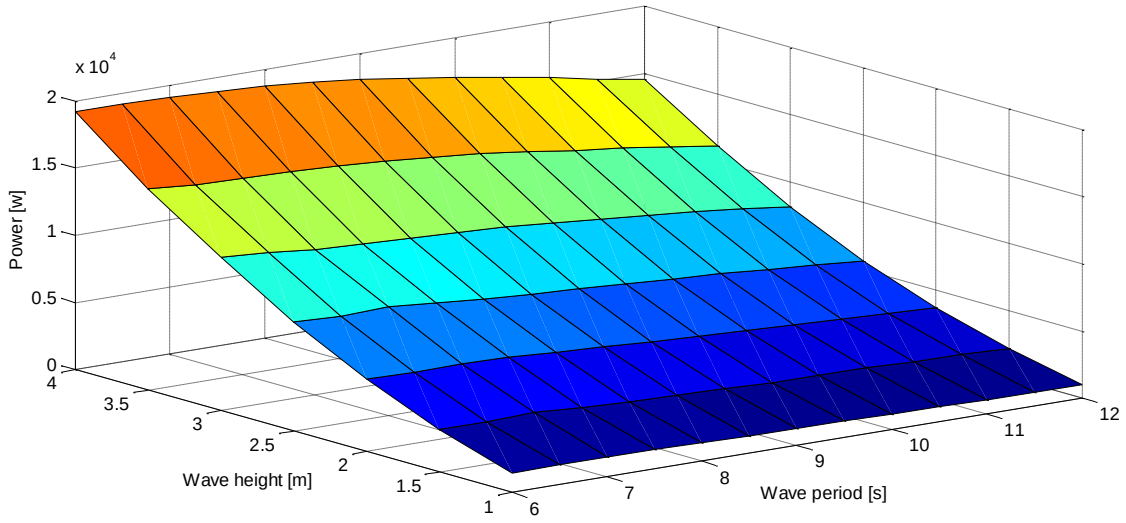

Figure 3. Power variation [W] for regular waves assuming DW.

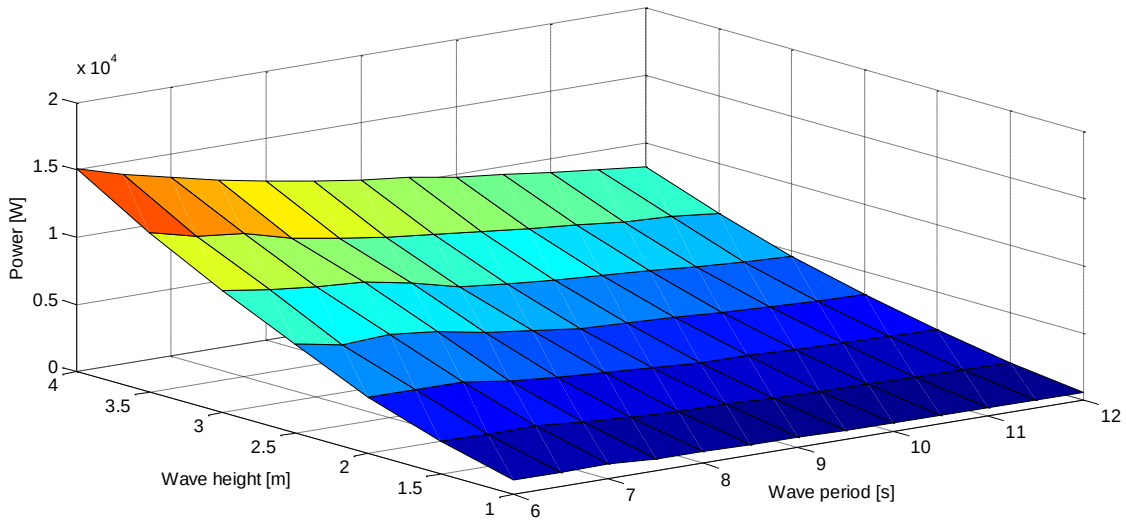

Figure 4. Power variation [W] for regular waves assuming IWD.

From Figures 3 and 4 it can be seen that, irrespective of assuming DW or IWD, power increases with higher wave heights. The wave period seems not to affect the power evolution. Also, the evolution profile is similar in both, even if higher values where obtained for the DW assumption.

Figure 5 shows, for the same regular waves, the existing power variation difference between DW and IWD assumptions.

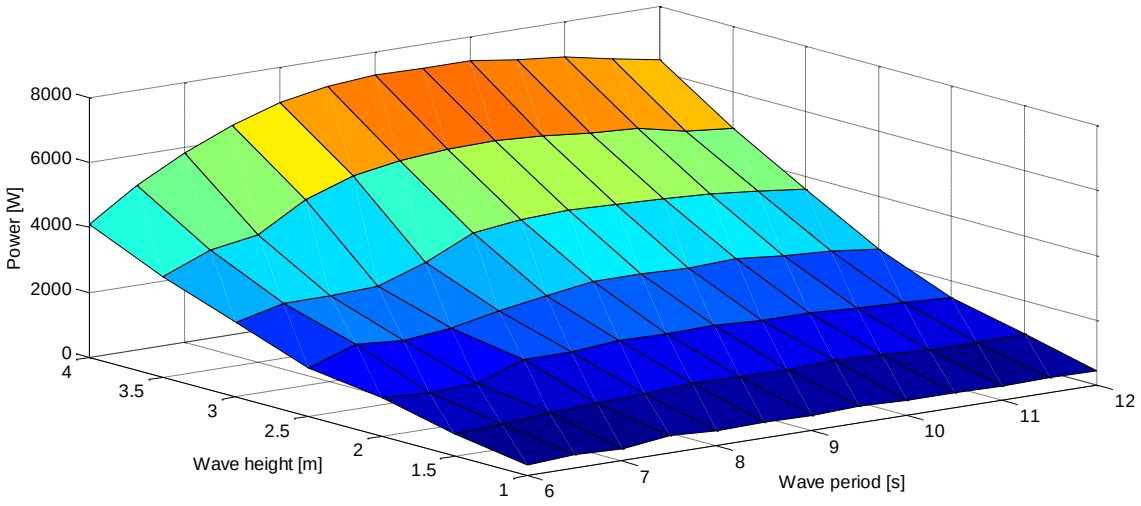

Figure 5. Difference in power variation [W] for regular waves assuming DW and IWD.

Figures 6 to 11 detail the time evolution of two regular waves, with H = 2 m; T_w = 8 s and H = 1.5 m; T_w = 10 s, respectively. Those values are within the regular wave range given in section 4. For a better comprehension, only a 50 seconds detail of the time evolution will be shown in some of the following figures.

Figure 6 shows the time evolution of regular wave with parameters H = 2 m; T_w = 8 s together with corresponding buoy displacement. Four curves are displayed, grouped in two pairs according with the respective RDC: IWD wave (green dot curve) together with the matching IWD buoy displacement (blue solid curve) and DW wave (red dash curve) together with the matching DW buoy.

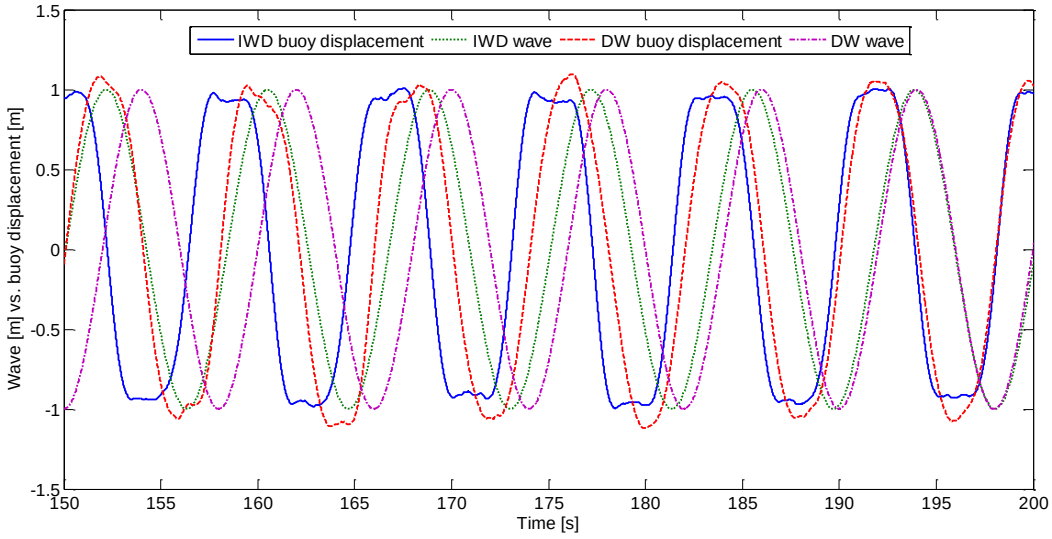

Figure 6. Time evolution [s] of regular wave vs. buoy displacement [m].

Figure 7 shows, for the same regular wave parameters, the time evolution of the excitation force together with corresponding buoy velocity. As above, four curves are displayed, grouped in two pairs according with the respective RDC: IWD excitation force (green dot curve) together with the matching IWD buoy velocity (blue solid curve) and DW excitation force (red dash curve) together with the matching DW buoy velocity (purple dash-dot curve).

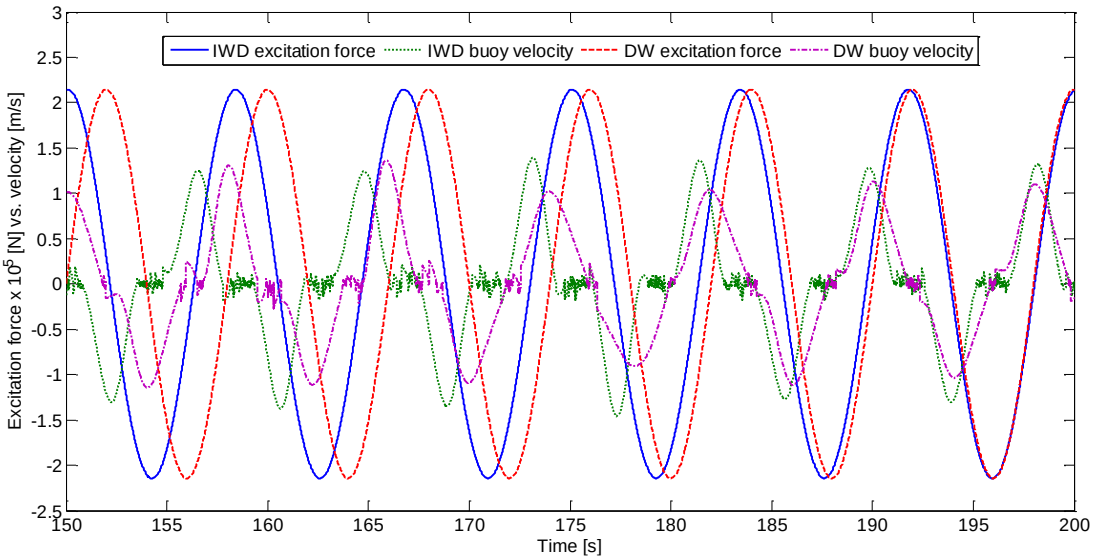

Figure 7. Time evolution [s] of excitation force × 10^5 [N] vs. buoy velocity [m/s].

Figure 8 shows, for the same regular wave parameters, the time evolution of the energy supplied by the ELG. Two curves are displayed: one assumes IWD (blue solid curve) and other considers DW (red dash curve).

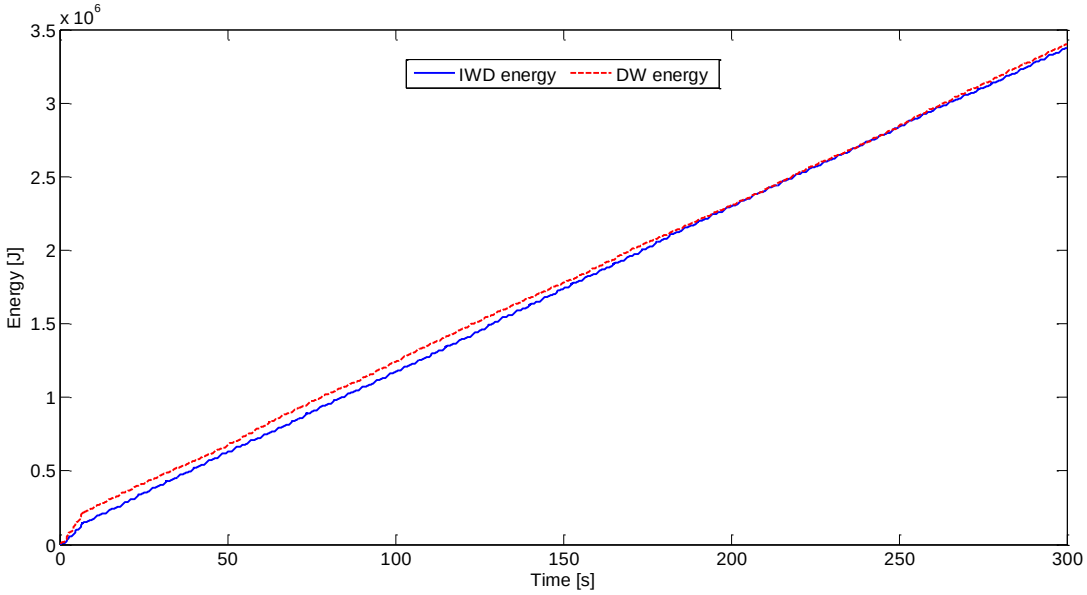

Figure 8. Time evolution of ELG energy [J].

Figures 9 to 11 show the same as Figures 6 to 8, but for the second regular wave mentioned above (H = 1.5 m; T_w = 10 s).

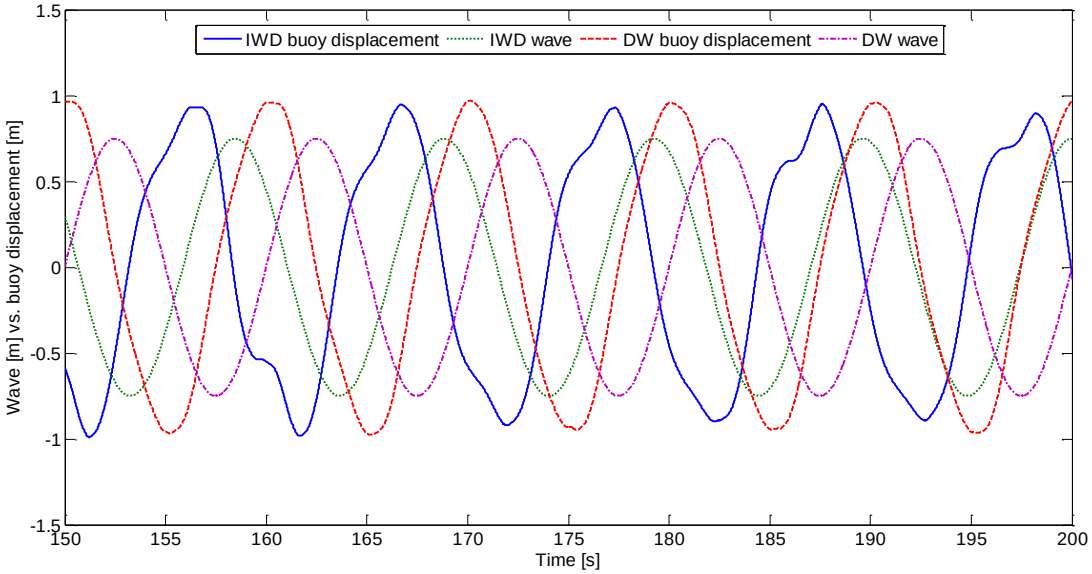

Figure 9. Time evolution [s] of regular wave vs. buoy displacement [m].

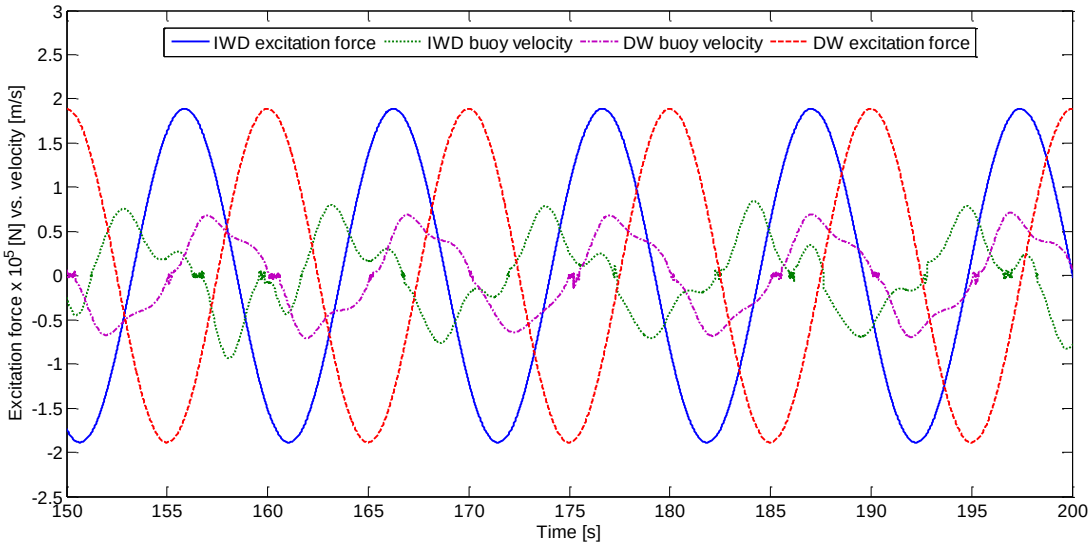

Figure 10. Time evolution [s] of excitation force × 10^5 [N] vs. buoy velocity [m/s].

Results presented in Figures 6, 7, 9 and 10 reveal that oscillating variables are all out of phase, which is a direct consequence of equations (7) and (10). If that could be eliminated the curves would match quite reasonably. The peak-to-peak amplitude of the same oscillating variables does not seem to be affected by the depth effect (simulated by the two different RDC values used) since maximum values remain rather close.

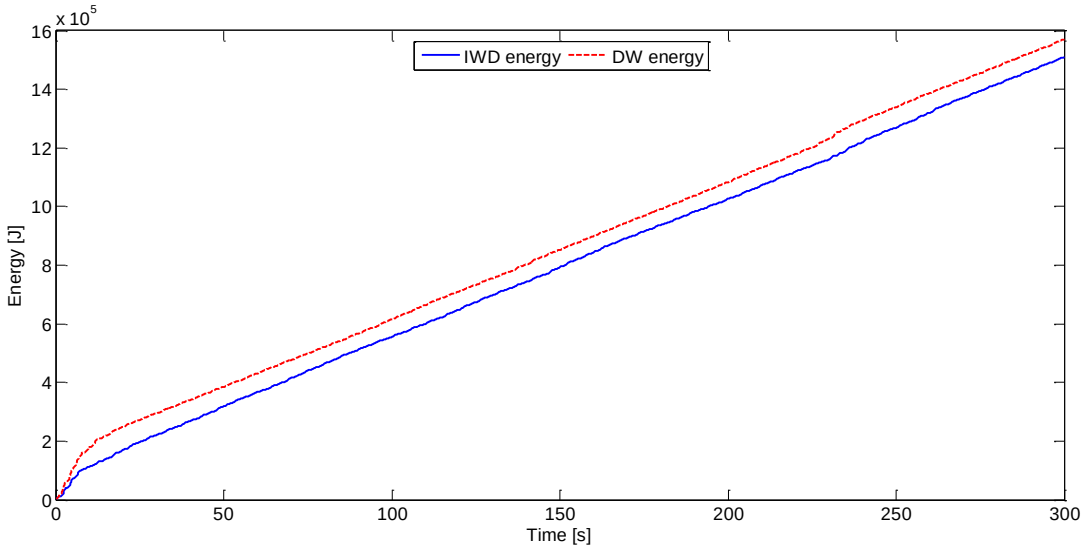

Figure 11. Time evolution of ELG [J].

From Figures 8 and 11 it can be seen that there are no noticeable differences between the energy values calculated for RCD = 0.25 (assuming IWD) and RCD = 1 (assuming DW), even though a different value is obtained for the energy delivered before the transient regime is reached. Still higher values are obtained for the DW assumption, confirming results depicted in Figures 3 and 4.

However the most important result is that the power that the ELG can supply is similar when the RCD triggers the selection between DW and IWD formulation.

Thus, when dealing with a WEC classified as an IWD device, the corresponding more complex IWD equations described in section 3 for the fluid velocity w, wave angular frequency ω, wavelength λ and radiation force f_r can be replaced by their analogous simpler DW equations without the danger of committing significant errors.

6.2. Irregular waves

Recalling Table 1 in section 4, twelve sea states (one for each month of the year), were used to perform several simulations, again using the TDS. Simulation results obtained for one of those irregular waves (corresponding to March) are presented in Figures 12 to 14. Plots include the same oscillating variables already depicted in the analysis performed for the regular waves. Like in the regular waves presented above only a 50 seconds detail of the time evolution will be shown in Figures 12 and 13.

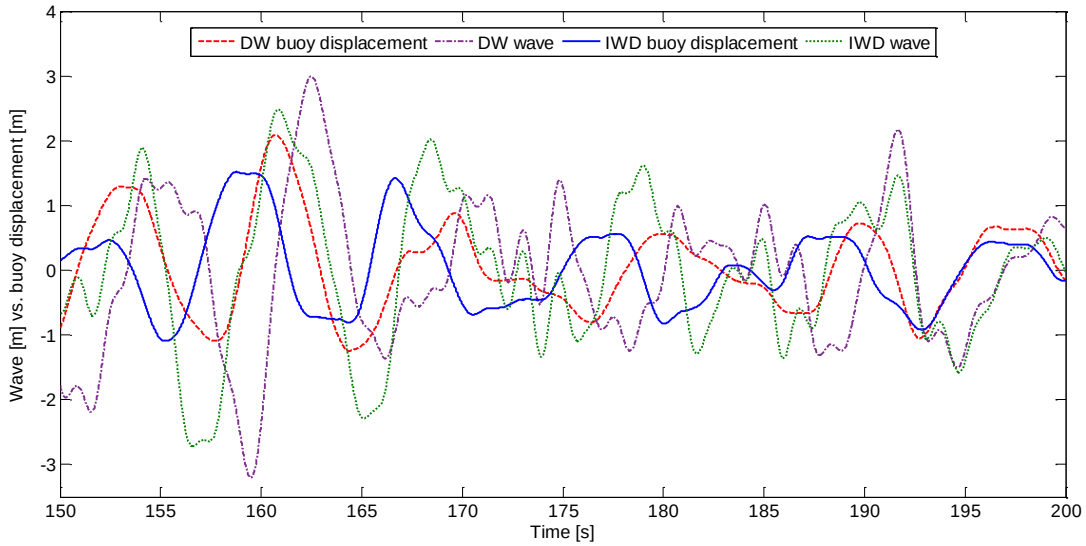

Figure 12. Time evolution [s] of irregular wave vs. buoy displacement [m].

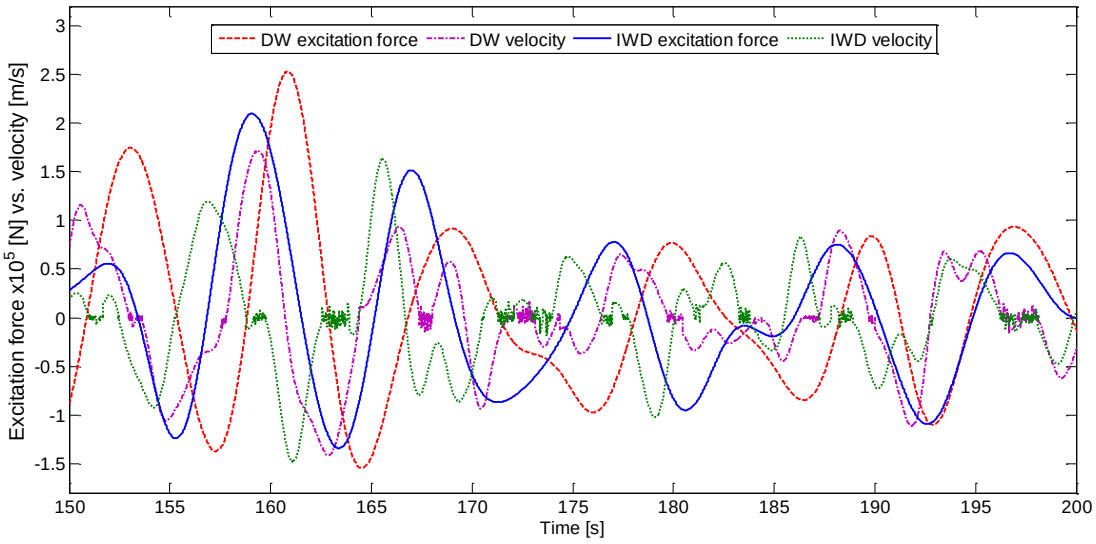

Figure 13. Time evolution [s] of excitation force × 10^5 [N] vs. velocity [m/s].

Figure 14 shows, for the irregular wave of March, the time evolution of the energy supplied by the ELG. Two curves are displayed: the blue solid curve refers to IWD and the red dash curve states for DW formulation.

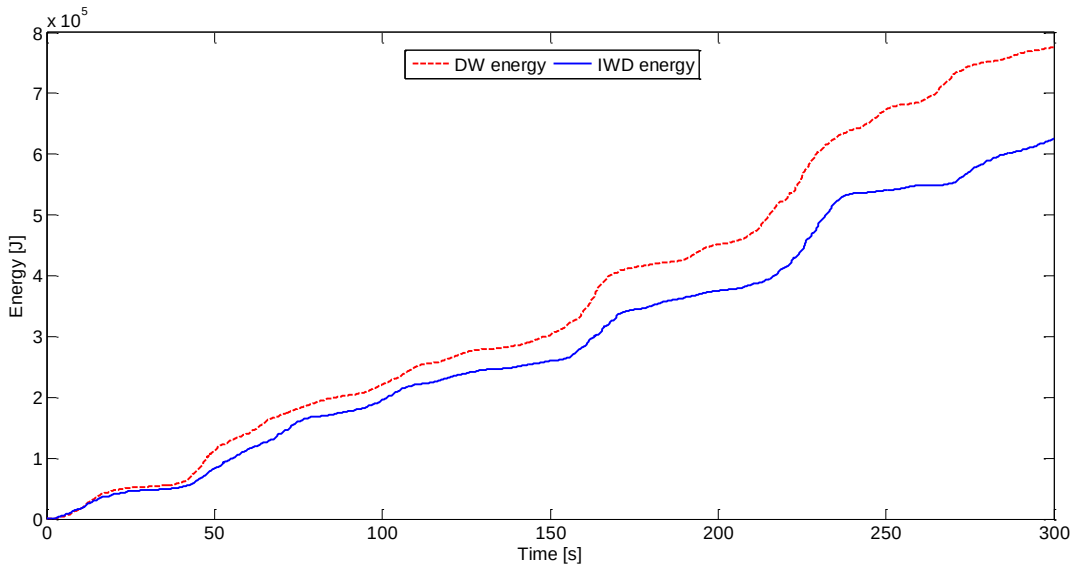

Figure 14. Time evolution of ELG [J].

Figure 14 shows that higher energy values are obtained for the DW formulation, confirming results already obtained for the regular waves. Again it can be seen that there are no noticeable differences between values calculated for DW and IWD.

Figure 15 illustrates the power obtained for the twelve irregular waves assuming DW and IWD formulation respectively.

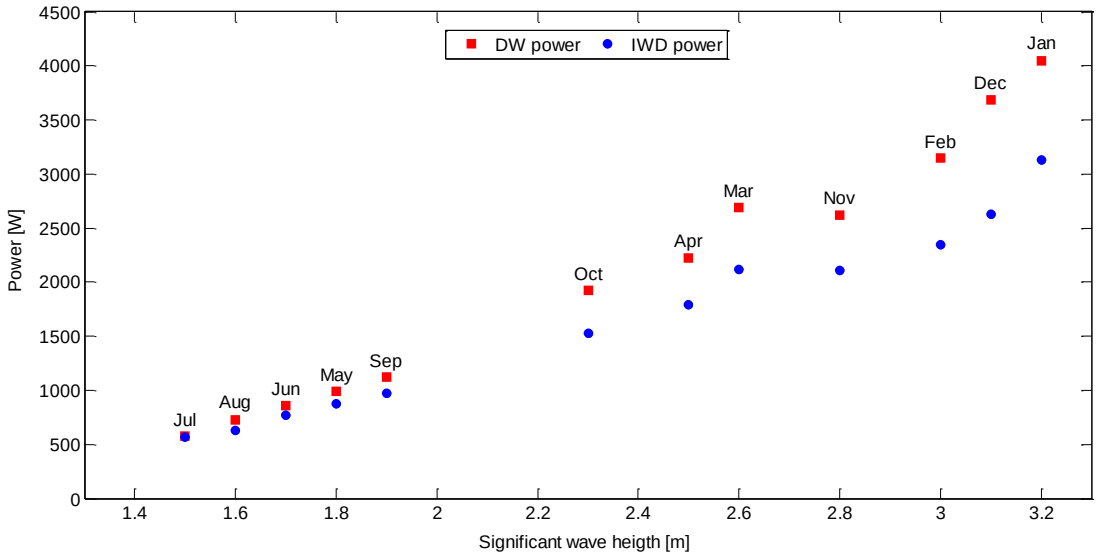

Figure 15. Power obtained for several sea states assuming DW and IWD.

It can be seen that, as for regular waves, the DW assumption always leads to higher power values. Also the difference in the power values between IWD and DW formulation increases with the increase of the significant wave height H_s. The difference is negligible for the so-called summer months, being higher for the so-called winter months.

7. Conclusion

This paper describes and compares, by means of simulations, eventual differences in the power that can be captured by the device when DW and IWD are assumed. Actually there are several parameters, described by mathematical equations presented here, that are affected by these two formulations. These parameters can also affect others and eventually an error can be propagated. Therefore it seems important to seek if the error, caused when more complex IWD equations are replaced by simple DW equations, can be neglected.

The RDC is responsible by the selection between DW and IWD equations respectively. The development of a mathematical model with specific equations for the usual DW assumption as well as for IWD was also described.

Numerical results obtained by means of simulations reveal that the computed power is higher when DW formulation is used; this conclusion stands for both regular and irregular waves.

Considering regular waves and specifically waves with higher heights and lower periods the power also increases when DW formulation is used instead of IWD (this can be seen from Figures 3 and 4). For lower wave heights the wave power seems to be independent of the wave period and of DW or IWD assumptions (this can also be seen from Figures 3 and 4).

Considering irregular waves, the power computed, for less energetic sea states (so-called summer months on northern hemisphere), is independent of DW or IWD formulations. For higher energetic sea states (so-called winter months in the same hemisphere) the power gain can be up to 40% when DW formulation is assumed. The wave period does not affect power since Pierson-Moskowitz spectrum is independent of this parameter. Thus, the more complex IWD equations can be replaced by their corresponding and simpler DW equations without the danger of committing significant errors if the wave height stays below a given value, since numerical results obtained by means of simulations point out that there are no relevant differences between those two assumptions.

Conflict of Interest

All authors declare no conflicts of interest.

References

1. Li Y, Yu Y-H (2012) A synthesis of numerical methods for modeling wave energy converter-point absorbers. *Renew Sustain Energy Rev* 16: 4352-4364
2. Falcão A (2010) Wave Energy Utilization: A Review of the Technologies. *Renew Sustain Energy Rev* 14: 899-918.
3. Falnes J (2007) A review of wave-energy extraction. *Mar Struct* 20: 185-201.
4. Fernandes A, Fonseca N (2013) Finite depth effects on the wave energy resource and the energy captured by a point absorber. *Ocean Eng* 67: 13-26.
5. Nieuwkoop-McCall J, Smith H, Smith G, Edwards K, Effect of water depth on the wave energy resource and extreme wave conditions. 4th International Conference on Ocean Energy; 2012 Oct 17, Dublin, Ireland.
6. Folley M, Whittaker T (2009) Analysis of the nearshore wave energy resource. *Renew Energy* 34: 1709-1715.

7. Stratigaki V, Troch P, Stallard T, et al. (2014) Wave Basin Experiments with Large Wave Energy Converter Arrays to Study Interactions between the Converters and Effects on Other Users in the Sea and the Coastal Area. *Energies* 7: 701-734.
8. Falnes J (2002) *Ocean Waves and Oscillating Systems: Linear Interactions Including Wave-Energy Extraction*, 1 Eds., Cambridge: Cambridge University Press.
9. Drew B, Plummer A, Sahinkaya M (2009) A review of wave energy converter technology. *J Power Energy* 223: 887-902.
10. Prado M, Polinder H (2011) Direct Drive in Wave Energy Conversion–AWS Full Scale Prototype Case Study. IEEE Power and Energy Society General Meeting; 2011 July 24-29; Detroit, USA.
11. Beirão P, Malça C (2014) Design and analysis of buoy geometries for a wave energy converter. *Int J Energy Environ Eng* 5: 1-11.
12. Bozzi S, Miquel A, Antonini A, et al. (2013) Modeling of a Point Absorber for Energy Conversion in Italian Seas. *Energies* 6: 3033-3051.
13. Sarlak H, Seif M, Abbaspour M (2010) Experimental Investigation of Offshore Wave Buoy Performance. *J Mar Eng* 6: 1-11.
14. Tyrberg S, Waters R, Leijon M (2010) Wave power absorption as a function of water level and wave height: theory and experiment. *IEEE J Ocean Eng* 35: 558-564.
15. Biesheuvel A, Spoelstra S (1989) The added mass coefficient of a dispersion of cylindrical gas bubbles in liquid. *Int J Multiphase Flow* 15: 911-924.
16. Vu K, Chenu B, Thiagarajan K, Hydrodynamic Damping due to Porous Plates. WSEAS International Conference on Fluid Mechanics; 2004 Aug 17-19; Corfu, Greece.
17. U.S. Army Corps of Engineers: Water Wave Mechanics Coastal Engineering Manual (EM 1110-2-1100) U.S. Army Corps Engineers, 2002. Available from: http://smos.ntou.edu.tw/CEM.htm.
18. Eriksson M, Waters R, Svensson O, et al. (2007) Wave power absorption: Experiments in open sea and simulation. *J Appl Phys* 102: 084910.
19. Engström J, Kurupath V, Isberg J, et al. (2011) A resonant two body system for a point absorbing wave energy converter with direct driven linear generator. *J Appl Phys* 110: 124904.
20. Finnegan W, Meere M, Goggins J (2013) The wave excitation forces on a truncated vertical cylinder in water of infinite depth. *J Fluids Struct* 40: 201-213.
21. Falnes J, Bjarte-Larsson T (2006) Theoretical and Experimental Investigation of Wave Energy Conversion by a Phase-Controlled Heaving Body. *J Eng Marit Environ* 220: 175-183.
22. Thorburn K, Leijon M (2007) Farm size comparison with analytical model of linear generator wave energy converters. *Ocean Eng* 34: 908-916.
23. Pontes M, Aguiar R, Pires HO (2005) A nearshore wave energy atlas for Portugal. *J Offshore Mech Arctic Eng* 127: 249-255.
24. Valério D, Beirão P, Sá da Costa J (2007) Optimisation of wave energy extraction with the Archimedes Wave Swing. *Ocean Eng* 34: 2330-2344.
25. Valério D, Mendes M, Beirão P, et al. (2008) Identification and control of the AWS using neural network models. *Appl Ocean Res* 30: 178-188.
26. Nunes G, Valério D, Beirão P, et al. (2011) Modelling and control of a wave energy converter. *Renew Energy* 36: 1913-1921.
27. Malça C, Beirão P, Felismina R (2014) Influence of material selection on the structural behavior of a wave energy converter. *AIMS Energy* 1: 359-372.

28. Sá da Costa J, Sarmento A, Gardner F, Beirão P, Brito-Melo A, Time Domain Model of the AWS Wave Energy Converter. 6th European Wave and Tidal Energy Conference; 2005 Aug 30-Sep 2; Glasgow, United Kingdom.
29. Beirão P, Malça C, Dynamic simulation in the time domain of a wave energy converter. 5th International Congress of Energy and Environment Engineering and Management; 2013 Jul 17-19, Lisbon, Portugal.

AIMS Press